Role of cortical tension in bleb growth

Jean-Yves Tinevez[a,b,1], Ulrike Schulze[a,b,1,2], Guillaume Salbreux[c,1,3], Julia Roensch[a,b], Jean-François Joanny[c,4], and Ewa Paluch[a,b,4]

[a]Max Planck Institute of Molecular Cell Biology and Genetics, 01 307 Dresden, Germany; [b]International Institute of Molecular and Cell Biology, 02 109 Warsaw, Poland; and [c]Laboratoire Physico-Chimie Curie, Unité Mixte de Recherche 168, Institut Curie, Centre National de la Recherche Scientifique, University Paris VI, 75 005 Paris, France

Edited by Timothy J. Mitchison, Harvard University, Boston, MA, and accepted by the Editorial Board August 19, 2009 (received for review March 30, 2009)

Blebs are spherical membrane protrusions often observed during cell migration, cell spreading, cytokinesis, and apoptosis, both in cultured cells and in vivo. Bleb expansion is thought to be driven by the contractile actomyosin cortex, which generates hydrostatic pressure in the cytoplasm and can thus drive herniations of the plasma membrane. However, the role of cortical tension in bleb formation has not been directly tested, and despite the importance of blebbing, little is known about the mechanisms of bleb growth. In order to explore the link between cortical tension and bleb expansion, we induced bleb formation on cells with different tensions. Blebs were nucleated in a controlled manner by laser ablation of the cortex, mimicking endogenous bleb nucleation. Cortical tension was modified by treatments affecting the level of myosin activity or proteins regulating actin turnover. We show that there is a critical tension below which blebs cannot expand. Above this threshold, the maximal size of a bleb strongly depends on tension, and this dependence can be fitted with a model of the cortex as an active elastic material. Together, our observations and model allow us to relate bleb shape parameters to the underlying cellular mechanics and provide insights as to how bleb formation can be biochemically regulated during cell motility.

The cell cortex is a thin meshwork of actin filaments, myosin, and associated proteins that lies beneath the plasma membrane (1). Because of the presence of active myosin motors, which slide filaments with respect to one another in the network, the cortex is under tension. As a result, the cortex exerts pressure on the cytoplasm and can actively contract, driving cell deformations (2).

Blebs are spherical membrane protrusions that commonly occur at the cortex during cytokinesis, cell spreading, virus uptake, and apoptosis (3–7). Moreover, increasing evidence points to an essential role for blebs as leading edge protrusions during cell migration in three-dimensional environments, particularly during embryonic development and tumor-cell dissemination (8–11; reviewed in refs. 7, 12). Despite the importance of blebbing, very little is known about the mechanisms of bleb growth.

The life cycle of a bleb can be subdivided into three phases (7, 13). First, a bleb is nucleated, either by local detachment of the cortex from the plasma membrane or by local rupture of the cortex. In the subsequent growth phase, a membrane bulge, initially devoid of cortex, expands from the nucleation site. Finally, the cortex gradually reassembles at the bleb membrane, leading to bleb retraction.

Bleb formation is often correlated with high myosin II activity, and myosin II inhibition prevents blebbing (6, 7, 10, 14). For that reason, and because of their round shape and rapid expansion, blebs are commonly believed to be a direct mechanical consequence of the hydrostatic pressure exerted on the cytoplasm by the contractile cortex, which would drive bleb growth from places of local cortex weakening without any further regulation (7, 15, 16). However, this purely mechanical interpretation of blebbing mostly relies on indirect observations, and, to our knowledge, neither the mechanical nature of blebbing nor the link between cortex tension and bleb growth have ever been directly assessed. Moreover, a quantitative model describing the role of cortical tension in bleb expansion has not yet been established.

Here, we directly address the role of cortical tension in bleb growth by inducing bleb formation in cells with different tensions. We first show that blebs can be nucleated by local laser ablation of the actin cortex, supporting the view that bleb expansion is driven by intracellular pressure. Multiple ablations of the same cell indicate that the growth of a bleb significantly reduces pressure. We then modulate cortical tension and induce blebs in cells with different tensions. We demonstrate that there is a critical tension for bleb formation below which bleb growth cannot be induced. Above this threshold tension, bleb size increases with increasing tension. We fit our data with a theoretical model of the cortex as an elastic active gel. This model yields an estimate of cellular elasticity and gives an accurate prediction of bleb shape.

Results

Ablation of the Cell Cortex Leads to Bleb Formation. In order to test whether bleb formation is pressure-driven, we performed local laser-ablations of the cell cortex. We hypothesized that if bleb growth is a direct consequence of cytoplasmic pressure, a bleb would grow from the site of ablation. Conversely, if bleb formation requires further regulation, ablation should not immediately trigger bleb growth.

We chose L929 fibroblasts as a model system for our study: When in suspension, these cells display an active, continuous cortical layer under the plasma membrane (17). We therefore placed the detached fibroblasts in polyethylene glycol (PEG)-coated dishes, which prevent readhesion of cells to the substrate. By using a picosecond-pulsed 405-nm laser, we then locally ablated the cell cortex (Movies S1 and S2 in the *SI Appendix*). Strikingly, immediately after ablation, a bleb grew from the site of cortex disruption and reached its maximal size within 10-30 s (Fig. 1*A*). The bleb then remained stable for one to several minutes, followed by a retraction phase typically lasting over a minute (Movie S1 in the *SI Appendix*). We followed cortical dynamics after ablation in cells expressing myosin regulatory light chain (RLC)-GFP (Movie S2 in the *SI Appendix*); no myosin was initially present at the bleb membrane, and a myosin layer became clearly visible shortly before bleb retraction, similar to what is observed in spontaneously forming cellular blebs (13). Laser ablation thus appears to mimic the endogenous nucleation of blebs by local disruption of the cortex and supports the idea that bleb growth is driven by intracellular pressure.

Author contributions: J.-Y.T., U.S., G.S., J.-F.J., and E.P. designed research; J.-Y.T., U.S., G.S., J.R., J.-F.J., and E.P. performed research; J.-Y. T. and J.R. analyzed data; and J.-Y.T., G.S., J.-F.J., and E.P. wrote the paper.

The authors declare no conflict of interest.

This article is a PNAS Direct Submission. T.J.M. is a guest editor invited by the Editorial Board.

Freely available online through the PNAS open access option.

[1]J.-Y.T., U.S., and G.S. contributed equally to this work.

[2]Present address: European Molecular Biology Laboratory, Heidelberg, Germany.

[3]Present address: Department of Physics, University of Michigan, Ann Arbor, MI.

[4]To whom correspondence may be addressed. E-mail: jean-francois.joanny@curie.fr or paluch@mpi-cbg.de.

This article contains supporting information online at www.pnas.org/cgi/content/full/0903353106/DCSupplemental.

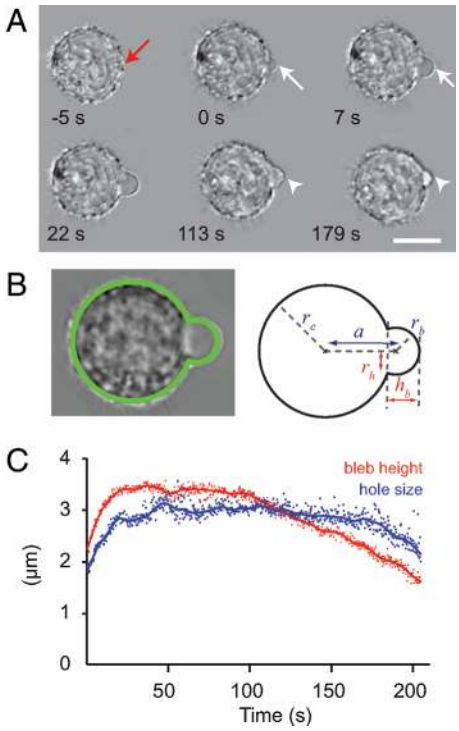

Fig. 1. Laser ablation of the cortex induces bleb growth. (*A*) Timelapse of a typical ablation movie. Ablation from −5 s to 0 s. Red arrow, site of ablation; white arrows, growing bleb; white arrowheads, retracting bleb. Scale bar, 10 μm. (*B*) Example of brightfield image analysis. The cell contour is fitted with two intersecting circles of radii r_c and r_b, with centers distant by a. r_h, hole size; h_b, bleb height. (*C*) Time course of bleb height (red) and hole size (blue) for a cell under control conditions (representative of $N = 37$ cells). *0 s*, offset of ablation. Dots are individual measurements (≈0.2 s/frame); lines are values smoothed over 10 points.

We then analyzed bleb shape over time by using transmitted light images (see Fig. 1 *B* and *C* and *Supplementary Materials and Methods* in the *SI Appendix*). The maximal volume reached by the bleb ranged between 0.3% and 6% of the cell volume ($2.73 \pm 0.23\%$, mean ± SEM, $N = 37$), and the bleb height ranged from 1.4 to 4.5 μm (3.45 ± 0.11 μm). The size of the bleb did not depend on the site of ablation with respect to the nucleus (Fig. S1 of the *SI Appendix*).

Bleb Growth Releases Cytoplasmic Pressure. To evaluate whether the growth of a bleb actually releases pressure, we performed multiple ablations on the same cell. Indeed, if the expansion of a bleb reduces intracellular pressure, a second bleb induced shortly afterward should reach a smaller size.

Therefore, we performed experiments where two blebs were sequentially triggered at opposite sides of a cell (Fig. 2*A*). We found that when the second ablation immediately followed the first one, the second bleb was significantly smaller than the first, whereas for ablations performed after the first bleb had retracted, no significant difference between the two bleb sizes was found (Fig. 2*B*). These observations suggest that the growth of a bleb significantly releases intracellular pressure and that pressure returns to its initial value once the bleb has retracted.

To assess whether the pressure release was homogenous throughout the cell or whether a pressure gradient was present, we induced the growth of a second bleb at various distances from the first one. The average decrease in size between the first and the second bleb was the same, regardless of whether the second bleb was nucleated close to or far from the first one (Fig. 2). This finding supports the view that pressure equilibrates fast when compared with the time scales of bleb expansion in this cell type.

It has been proposed that the pressure driving bleb growth is hydrostatic, resulting from tension built up in the actin cortex (7, 15). However, this pressure could also be of osmotic origin (18). We therefore sought to test the link between bleb expansion and cortical tension.

Myosin Activity and Actin-Binding Proteins Affect Cortical Tension. In order to identify factors likely to affect cortical tension, we developed a theoretical model of the cortex by using the hydrodynamic active gel theory (19, 20) (see *SI Appendix*). Within this framework, cortical tension is equal to $\zeta \Delta\mu h/2$ where $\zeta \Delta\mu$ is the active stress exerted by the myosins in the cortical gel, and h is the thickness of the cortex.

We then sought to experimentally modify cortical tension. Tension was measured by using micropipette aspiration (21, 22) (Fig. 3*A*). Under control conditions, L929 cells had a well-defined tension of 413.6 ± 15.2 pN/μm (mean ± *SEM*, $N = 32$, Fig. 3*B* and Table S1). Provided that the cortex is tightly coupled to the membrane, the tension measured by micropipette aspiration, T, is the sum of the active cortical tension and of the membrane tension γ. In order to estimate γ, we measured the tension of cells where the cortex had been disassembled with cytochalasin D (CD). Under these conditions, tension dropped to 39.1 ± 4.2 pN/μm ($N = 13$, Fig. 3*C*).

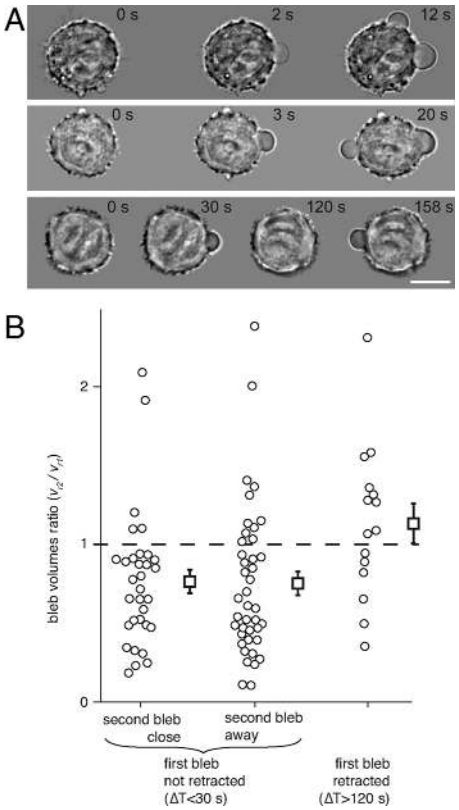

Fig. 2. Multiple ablations on the same cell lead to smaller blebs. (*A*) Time lapses from double-bleb experiments. (*Top* and *Middle*) Case 1: The second bleb is nucleated shortly after the first one (delay $\Delta T < 30$ s), either close to it (*Top*) or at the opposite side of the cell (*Middle*). (*Bottom*) Case 2: The second bleb is nucleated after the first bleb is fully retracted ($\Delta T > 2$ min). Scale bar: 10 μm. (*B*) Plot of the ratio of maximal bleb volumes (v_{r2}/v_{r1}) for case 1 and case 2. Open circles, single measurements; open squares, mean ± SEM. Case 1: The ratio of volumes is 0.76 ± 0.07 (mean ± SEM) for blebs induced close to one another and 0.75 ± 0.08 for blebs formed far from one another, and significantly differs from 1 ($P < 0.004$ and $P < 0.002$ respectively). Case 2: The volume ratio is 1.13 ± 0.13 and is not significantly different from 1 ($P > 0.3$). Cases 1 and 2 are significantly different ($P < 0.02$), whereas the two distributions of case 1 are not ($P > 0.9$).

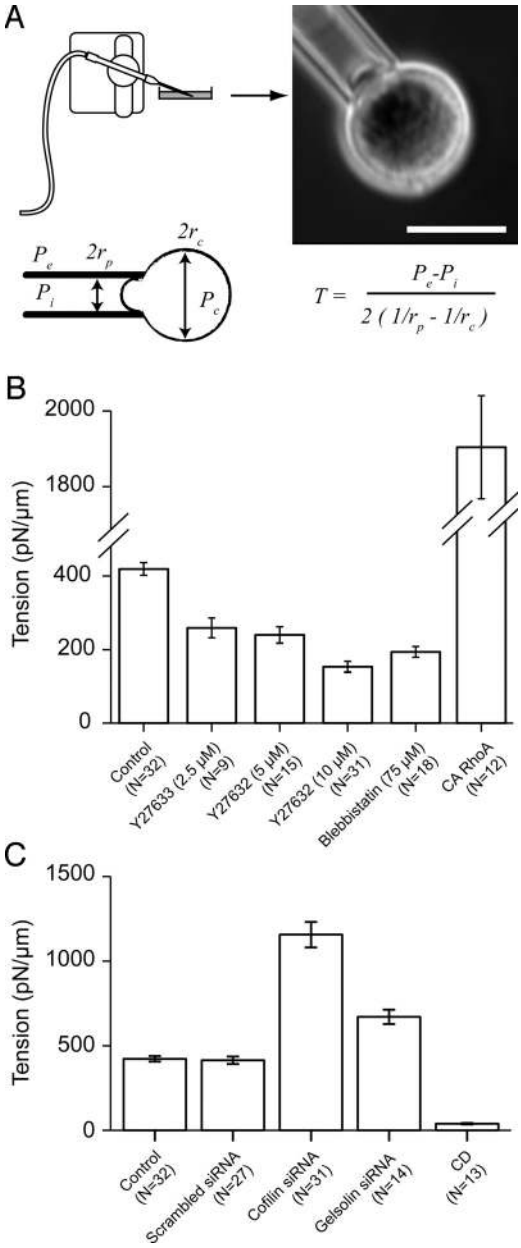

Fig. 3. Cortex tension depends on myosin activity and on proteins regulating actin turnover. (*A*) Schematic of the micropipette aspiration setup. The parameters used in the text and the formula used to calculate tension (Laplace law) are given. The image displays a detached L929 cell aspirated into a micropipette close to the critical pressure. Scale bar, 10 μm. (*B*) Cortex tension after treatments affecting myosin activity. (*N*: number of cells measured in 2–5 independent experiments). All groups were found to be significantly different from one another (two-sampled t-tests, $P < 0.05$), except for Y27632 2.5 μM versus Y27632 5 μM ($P = 0.36$), and Y27632 10 μM versus Blebbistatin ($P = 0.08$). (*C*) Cortex tension after treatments affecting actin. All groups were found to be significantly different from one another, except for control versus scrambled siRNA ($P = 0.77$). Protein depletion was checked by Western blotting (Fig. S4 in the *SI Appendix*).

We then measured cortex tension after various treatments affecting myosin II activity. Inhibition of myosin with blebbistatin decreased tension by more than 50% (Fig. 3*B*). Interestingly, we could gradually decrease tension by treating the cells with increasing amounts of Y27632, which indirectly reduces myosin activity by inhibiting Rho-kinase (ROCK)(23) (Fig. 3*B* and Table S1 of the *SI Appendix*). Finally, transfection with RhoAQ63L, a constitutively active version of the small GTPase RhoA (CA RhoA), an activator of myosin II (23), considerably increased tension to 1907.1 ± 140.7 pN/μm (Fig. 3*B*).

To assess the predicted dependence of tension on the thickness of the actin cortex, we then tested the influence of proteins involved in actin turnover. In addition to activating myosin II, RhoA can also enhance actin polymerization by activating formins (24); therefore, the increase in tension observed upon transfection with CA RhoA could result from the combined effect of a thicker cortex and higher myosin activity. We then investigated the effect of two proteins that regulate actin but are not involved in myosin regulation: actin depolymerizing factor (ADF)/cofilin, and gelsolin. Both depletion of gelsolin and cofilin by RNAi significantly increased the tension of L929 cells (Fig. 3*C*).

Bleb Size and Growth Dynamics Depend on Cortical Tension. We then analyzed the maximal size of blebs induced by laser ablation on cells with different tensions. Blebs induced on cells treated with CA RhoA or after cofilin depletion were bigger than blebs formed in control cells (Fig. S6 of the *SI Appendix*). However, as these treatments are likely to affect parameters other than cortical tension alone, we focused further analysis on cells treated with various amounts of the ROCK inhibitor Y27632.

We found that for tensions lower than 200 pN/μm (cells treated with 10 μM Y27632), blebs could not be induced. At 240 pN/μm, approximately 50% of the cells formed a bleb upon ablation, but the bleb volume was eight times smaller than in control situations. For higher tensions, all cells formed a bleb, and the bleb-to-cell volume ratio, the height of the bleb, and the maximal size of the hole at the base of the bleb all increased with increasing tension (Fig. 4 *A* and *B* and Fig. S2 and Table S1 of the *SI Appendix*). These data indicate that there is a threshold tension for bleb formation between 200 and 240 pN/μm. Above this threshold, bleb size increases with increasing tension.

We then asked whether the dynamics of bleb expansion also depended on cortical tension. The initial speed of bleb growth

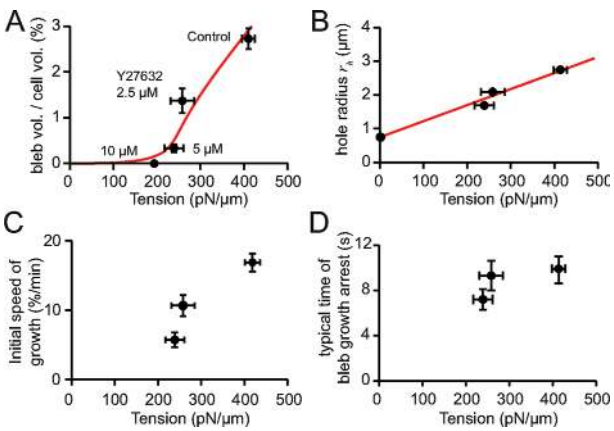

Fig. 4. Dependence of bleb size and growth dynamics on tension. Plots of bleb parameters for cells treated with Y27632 and control conditions and reported as function of the corresponding tension. In *B*, *C*, and *D* there is no data point for 10 μM Y27632, because a bleb could not be induced for this condition. Values displayed: mean ± SEM unless otherwise indicated. Plots of the maximal bleb-to-cell volume ratio (*A*), and hole size at maximal volume ratio (*B*) as a function of tension. Red curves, fits of the elastic model with two free parameters the cytoplasmic elasticity $\frac{E_i}{1-2\nu_i}$ and the effective cortex elastic modulus $E_c h$. The fit yields $E_c h = 240$ pN/μm, and $\frac{E_i}{1-2\nu_i} = 6,750$ Pa. The data point for $T = 0$ in *B* was used in the fitting and represents an estimate of the size of the hole made by laser ablation. (*C*) Initial speed of bleb growth, calculated as the rate of the time course of the bleb-to-cell volume ratio during the first 20 time points (7 to 12 s) after ablation. (*D*) Characteristic time for bleb growth arrest, calculated from the slope of the relation between the maximal bleb-to-cell volume ratio and the initial speed of growth. Vertical error bars, 95% confidence interval for this frame. The points were not found to be significantly different from one another.

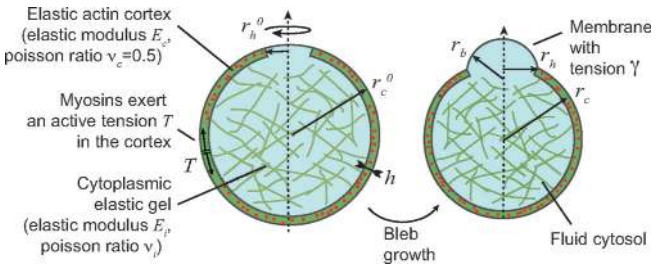

Fig. 5. Elastic model of bleb growth. Schematic of the mechanical elements involved in the Model of bleb expansion: Myosins in the cortex exert a tension that is responsible for cell contraction, expulsion of fluid cytosol into the bleb, and hole opening. The inner cytoplasmic gel and the cortex are then elastically compressed and therefore oppose cortical contraction. We assume cylindrical symmetry around the cell-bleb axis, as indicated by the curved arrow.

strongly increased with increasing tension (Fig. 4*C*). By plotting the maximal bleb-to-cell volume ratio as a function of the initial expansion speed, we also extracted the typical time scale of bleb growth arrest (Table S1 of the *SI Appendix*). This time did not significantly depend on tension (Fig. 4*D*), suggesting that growth arrest may result from a tension-independent mechanism.

Elastic Model for Bleb Growth. ***Description of the Model.*** We modeled bleb expansion as a result of the cytoplasmic pressure generated by cortical tension. Before bleb formation, intracellular pressure is given by Laplace's law $P_c = P_e + 2T/r_c$, where r_c is the radius of the cell and P_e is the pressure in the medium. If we neglect any elastic effect, P_c would still be given by Laplace's law during bleb growth, and would thus remain very close to its initial value because the radius of the cell decreases by less than 2% during bleb expansion. However, multiple ablation experiments indicate that intracellular pressure is significantly reduced during the growth of a bleb (Fig. 2).

To account for this pressure release, we incorporated the elasticity of cellular components in our description: The actin cortical gel has a Young modulus E_c, and the cytoplasm has a Young modulus E_i (Fig. 5). Indeed, the cytoplasm contains fluid cytosol, but it also contains membrane structures and cytoskeletal polymers, which are likely to have elastic properties (25). As a first approximation, we neglected turnover in the actin cortex on the time scale of bleb formation, and we considered that the cortex was incompressible (i.e., the Poisson ratio of the cortex $\nu_c = 0.5$). The cytoplasmic elastic gel, however, must be compressible to allow for the expansion of the bleb, so that the cytoplasmic Poisson ratio $\nu_i \neq 0.5$. Finally, we assumed that the total surface of the cell can change but its volume remains constant (see *Discussion*) and that the membrane of the bleb is devoid of cortex throughout the expansion of the bleb, as suggested by previous work (11, 26).

Bleb volume as a function of cortical tension. In our description, the bleb reaches its maximal volume at mechanical equilibrium, when the pressure of the cytosol inside the bleb equals the pressure inside the cell. Because we assume volume conservation, as the bleb grows the volume of the cell body decreases, compressing the cytoplasm and the actin cortex. The pressure of the cytosol in the cell body is therefore given by the pressure imposed by cortical tension $\frac{2T}{r_c}$, minus the elastic resistance of cellular structures. The resistance is proportional to the deformation of the cell and to the total elasticity of the cytoplasm and of the cortex. The pressure in the bleb is imposed by the membrane tension, yielding $P_b = 2\gamma/r_b$. Mechanical equilibrium is achieved when the two pressures are equal:

$$\frac{2T}{r_c} - \left(\frac{E_i}{1-2\nu_i} + 4E_c\frac{h}{r_c}\right)\frac{\Delta r_c}{r_c} = \frac{2\gamma}{r_b}, \qquad [1]$$

where Δr_c is the variation of the cell radius due to bleb formation (see *SI Appendix* for detailed derivation). Δr_c can be related to the bleb volume, and one obtains from Eq. **1** a relationship between the equilibrium bleb-to-cell volume ratio and the cortical tension, which can be accurately fitted to the experimental data with a single adjustable parameter, the total elasticity $(\frac{E_i}{1-2\nu_i}+4E_c\frac{h}{r_c}) \simeq 6850$ Pa ($R^2 = 0.91$, Fig. 4*A*), taking $r_c = 8.5$ μm and $\gamma = 40$ pN/μm.

Strikingly, the theory predicts the existence of a threshold tension for the expansion of a bleb, as observed experimentally (Fig. 4*A*). Qualitatively, the threshold results from the finite tension of the membrane. Indeed, two regimes can be distinguished, depending on whether membrane tension can resist bleb expansion. The maximal pressure reached in the bleb is on the order of $2\gamma/r_h$, where r_h is the size of the hole at the base of the bleb: At intracellular pressures lower than this value, the plasma membrane limits bleb growth and the volume of the bleb remains very small; for higher intracellular pressures, the pressure in the bleb becomes negligible, bleb growth is only limited by cellular elasticity, and the bleb becomes much larger. The critical pressure for bleb expansion is therefore roughly given by $T_c \sim \gamma r_c/r_h$. With $r_h \sim 1$ μm, $r_c \sim 8$ μm and $\gamma \sim 40$ pN/μm, this qualitative argument yields $T_c \sim 320$ pN/μm. The exact calculation, taking into account that r_h depends on tension (Fig. 4*B*), gives $T_c \sim 200$ pN/μm, in remarkable agreement with the experimental observations (Fig. 4*A*).

Size of the hole in the cortex as a function of cortical tension. To evaluate the surface elasticity of the cortex $E_c h$, we then modeled the opening of the hole at the base of the bleb, which is driven by cortical tension and is resisted by the elasticity of the cortex. We therefore calculated the deformation of the cytoplasmic gel and actin cortex during bleb growth (see *SI Appendix*) and found that the elasticity of the cytoplasm is essential to account for the observations. Indeed, in the limit where cytoplasmic elasticity is neglected ($E_c\frac{h}{r_c} \gg \frac{E_i}{1-2\nu_i}$), the maximal opening of the hole Δr_h is on the order of $r_c\frac{\gamma}{E_c h}$. In this limit, estimating $E_c h$ from the fit for the bleb volume (Fig. 4*A*), we obtain $\Delta r_h \simeq 50$ nm, which is far too small to account for the experimental data (Fig. 4*B*). In the opposite limit, where the elastic response is dominated by the compressibility of the cytoplasm ($E_c\frac{h}{r_c} \ll \frac{E_i}{1-2\nu_i}$), the maximal opening of the hole is proportional to the tension $\Delta r_h = \frac{3T}{2E_c h}r_h^0$, where $r_h^0 \simeq 0.75$ μm is the initial hole radius (see *Materials and Methods*). Fitting the experimental data gives $E_c h \simeq 240$ pN/μm (Fig. 4*B*, $R^2 = 0.99$). From the fit of Fig. 4*A*, we then obtain the cytoplasmic compressibility $\frac{E_i}{1-2\nu_i} = 6750$ Pa, consistent with our assumption $E_c\frac{h}{r_c} \ll \frac{E_i}{1-2\nu_i}$ because $h \ll r_c$.

Discussion

Laser Ablation Mimics Endogenous Nucleation of Blebs. We have shown that local ablation of the actin cortex leads to the formation of a membrane bleb (Fig. 1*A*). The artificially nucleated blebs appeared identical to the blebs naturally occurring in cells (13). The induced blebs were spherical in shape and mostly devoid of intracellular structures (Movie S1 of the *SI Appendix*). Growth and retraction times were similar to those measured on blebs forming spontaneously (ref. 26 and Table S1 and Movie S1 of the *SI Appendix*). Moreover, myosin reassembled at the bleb membrane shortly before bleb retraction (Movie S2 of the *SI Appendix*), similar to previous observations in spontaneously blebbing cells (13). Taken together, these observations indicate that laser ablation mimics endogenous bleb nucleation by local disruption of the cortex.

Cortex Tension Depends on Motor Activity and on Actin Turnover. Suspended L929 fibroblasts had a tension of ~413 pN/μm (Fig. 3*B*), similar to tensions measured in other fibroblast lines (27).

Tension measurements after actin disassembly with CD give an estimation of the membrane tension: $\gamma \sim 40$ pN/μm. This value is about 100 times higher than the typical membrane tension of a lipid vesicle (28) but comparable with the cortical tension of red blood cells (21), consistent with the observation that an erythrocytic-like cytoskeleton is observed at the plasma membrane of mammalian cells even during the expansion of blebs, when the actin cortex is absent (13).

We then showed that cortical tension of L929 fibroblasts strongly depends on myosin activity (Fig. 3*B*), in agreement with previous observations in *Dictyostelium discoideum* cells (29–31), where myosin II and several variants of myosin I are implicated in cortical tension. Importantly, we also showed that cortex tension depends on the level of proteins regulating actin turnover. Indeed, depletion of cofilin and gelsolin both resulted in an increase of cortical tension. ADF/cofilin enhances the rate of actin depolymerization and severs actin filaments (32); gelsolin also severs actin filaments and can moreover cap F-actin barbed ends, preventing further polymerization (33). Depletion of gelsolin or cofilin is therefore likely to result in a thicker actin cortex, which, in accordance with our model, should result in a higher tension, as observed experimentally (Fig. 3*C*). A tight control of cortical tension is likely to be essential during cell motility (2), but it is also essential in tissues, where differences in cortex tensions between cell types have been shown to contribute to cell sorting (34). The mechanisms of tension regulation are still largely unknown; our results show that studies of tension regulation cannot be limited to the action of myosin motors but should also include an analysis of actin turnover.

Above a Critical Tension, Bleb Size Increases with Increasing Tension. We show that both size and growth speed of a bleb strongly depend on cortical tension (Fig. 4), and we propose a model where the growth of a bleb results from a flow of cytoplasm generated by contractions of the actomyosin cortex. The theoretical model predicts the existence of a threshold in tension for the expansion of a bleb, as observed experimentally (Fig. 4*A*). Moreover, the model accurately fits the experimentally observed dependence of bleb volume and hole radius on tension for cells treated with Y27632 (Fig. 4 *A* and *B*), yielding values of cellular parameters that are in good agreement with independent measurements of these parameters. Specifically, we find a value for the cortex effective elastic modulus $E_c h \simeq 240$ Pa.μm. The thickness of the cortex has not been accurately measured and is likely to vary between cell lines (35, 36); however, electron microscopy observations of the cortex in Hela fibroblasts suggest a cortical thickness of about 100 nm (13). By using this value, we then get $E_c \simeq 2{,}400$ Pa, in agreement with other measurements of cortex elasticity (37). The theory also predicts a cytoplasmic compressibility $\frac{E_i}{1-2\nu_i} = 6{,}750$ Pa. The elasticity of L929 cells after depolymerization of actin has been previously measured by AFM and gives an estimated value for $E_i \sim 1{,}200$ Pa (37). We can therefore deduce the compressibility of the cytoplasm: $\nu_i \sim 0.41$, consistent with previous measurements of compressibility of cytoskeletal networks (38).

Expression of CA RhoA and depletion of cofilin are likely to result in a thicker cortex and therefore increase cellular elasticity, which resists bleb expansion. In agreement with this prediction, the blebs obtained after these treatments were smaller than would be expected with the elastic parameters inferred above from the size of blebs induced after gradual inhibition of myosin activity (Fig. S6 of the *SI Appendix*).

Taken together, our findings indicate that the size of a cellular bleb results from the net effect of cortical tension, which drives the expansion of the bleb, and of cellular elasticity and membrane tension, which resist expansion. All these factors can be regulated independently, which can explain how cells such as *Dictyostelium*, which have a relatively high tension [up to 4,000 pN/μm (29)], do not form blebs bigger than about 10% of the cellular volume (39).

Discussion of the Model of Bleb Expansion. Our model considers the cortex as an elastic, contractile shell surrounding a poro-elastic, liquid-gel cytoplasm. Given that the suspended L929 cells are spherical, we consider that the cortex is isotropic, with homogenous thickness and tension.

We further assume that cytosolic pressure is homogenous. Previous work on blebbing cells suggests that the density of cytoplasmic structures can slow down pressure equilibration inside the cell sufficiently enough to give rise to pressure gradients on time scales of tens of seconds (25, 26). However, in L929 cells, we have observed that blebs formed near the nucleus, where we expect the cytoplasmic structures to be more crowded, and far from it had similar sizes (Fig. S1 of the *SI Appendix*). Moreover, experiments where two blebs were successively induced on the same cell showed that as early as 7 s after bleb initiation, the decrease in pressure due to the growth of the first bleb was independent of the distance between the blebs (Fig. 2). These observations support our assumption that in L929 cells, at time scales relevant for bleb expansion, pressure is homogenous throughout the cytoplasm.

A second assumption is that the total volume of the cell is conserved. Although the plasma membrane is permeable to water, the high osmolarity of the cell should theoretically maintain an approximately constant volume. Indeed, the total cell volume varies in order to satisfy the balance between the osmotic and hydrostatic pressures $\Pi_c - \Pi_e = P_c - P_e$, where Π_c and Π_e are the intracellular and external osmotic pressures (40). By using Van't Hoff's law, $\Pi_e = c_{\text{ext}} R\theta$, where $c_{\text{ext}} \sim 300$ mol/m^3 is the osmolarity of the medium, R is the gas constant, and θ is the temperature, we get $\Pi_e \sim 5.10^5 Pa$ and $\Pi_c = n_t R\theta / V_c$, where n_t is the total number of moles of osmolytes in the cell. The volume of the cell is then given by

$$V_c = \frac{n_t R\theta}{\Pi_e + P_c - P_e}. \qquad [2]$$

Pressure variation in the cell during bleb formation is necessarily smaller than the initial intracellular excess pressure $2T/R \sim 100\ Pa$, which is three orders of magnitude smaller than the osmotic pressure. By using Eq. **2**, if cellular osmolarity does not change during bleb growth, the total volume change would then not exceed $|\Delta V_c|/V_c \sim |\Delta P_c|/\Pi_e \sim 0.02\%$, which is negligible compared with the typical volume of the blebs induced by laser ablation.

It is also possible that the ablation induces a local uptake or release of ions, which could drive water uptake. We have therefore verified how our results would be affected by an increase of the cell volume upon ablation and found that the experimental results cannot be accurately fit in the presence of a significant volume variation, further supporting our hypothesis of conserved volume (see *SI Text* and Fig. S8 of the *SI Appendix*).

Finally, our model assumes that the bleb membrane is devoid of an actin cortex throughout bleb expansion, in accordance with previous observations (13). However, our observation that the characteristic time of bleb growth arrest does not depend on tension (Fig. 4*D*) suggests that a tension-independent mechanism may stop bleb expansion. Cortex reassembly at the bleb membrane could play such a role, as previously suggested for blebs formed by actively blebbing filamin-depleted cells (15). If bleb expansion is stalled by actin repolymerization, the maximal volume reached by the bleb will be smaller than the volume predicted by our steady-state calculation. In that case, the elastic moduli derived above would be an overestimation of the real values. A theoretical description of the dynamics of bleb expansion will be necessary to calculate the evolution of bleb size over time. In addition to cortical tension and cell elasticity, dissipation mechanisms,

such as flow of cytosol through the cytoplasmic network and friction between the membrane and the cortex, will also influence bleb size.

Implications of the Critical Tension for the Regulation of Bleb Formation. The existence of a critical tension for the expansion of a bleb has been previously hypothesized (16); however, to our knowledge, our data provide the first experimental evidence of such a threshold tension. This observation unveils a fundamental mechanism that can be used by cells for the regulation of blebbing. Indeed, regulation of bleb formation can be achieved by controlling either bleb nucleation or bleb expansion. Bleb nucleation will depend on the strength of cortex–membrane attachments and on cortex stability; we show that bleb expansion will only occur above a critical tension. It will be important to know at which level endogenous bleb formation is regulated, for example, in cells migrating by blebbing. Interestingly, reduction of cortical tension by down-regulation of myosin II can inhibit bleb-based migration (10, 11); however, as cortical tension could also be important for bleb nucleation (7), it is difficult to distinguish between the two potential regulation mechanisms. Mimicking bleb nucleation by laser ablation can be an interesting tool to figure out the level at which cellular blebbing is regulated.

Materials and Methods

Cell Preparation and Tension Measurements. Mouse L929 fibroblasts were grown in DMEM (GIBCO, Invitrogen) supplemented with 10% FCS, 1% glutamine, and 1% penicillin-streptomycin. For all the experiments, the cells were maintained in suspension on PEG-coated glass-bottom dishes (Matttek) (ref. 17; see *Supplementary Materials and Methods* in the *SI Appendix*). We checked that detachment did not induce apoptosis in L929 cells (Fig. S3 of the *SI Appendix*). Details on drug treatments, plasmids, RNAi, and transfection are given in the *Supplementary Materials and Methods* in the *SI Appendix*. Tensions were measured by micropipette aspiration, as described in ref. 21 (see *Supplementary Materials and Methods* in the *SI Appendix*).

Laser Ablation and Cell Imaging. Laser ablation experiments were performed on a scanning confocal microscope (Olympus FV1000) equipped with two scanning heads. The first one was used for standard imaging, and the second one was coupled to a laser head (LDH-P-C-405B, PicoQuant GmbH), driven by a power source (PDL 800-B, PicoQuant GmbH) delivering 405-nm picosecond pulses with a nominal power of 3 mW. For ablation, the pulsed laser was undergoing spiraling movements within a circle of 600 nm nominal diameter for 5 s. The actual ablation spot was around 1.5 μm in diameter, as estimated from fluorescence images immediately after ablation (Movie S2 of the *SI Appendix*). For fluorescence imaging, the pinhole size was set so as to have Z-sections of about 1 μm, thickness. For transmitted light imaging, a 561-nm laser was used as a light source. Because the ablation laser saturated the transmitted light detector, transmitted images could not be acquired during ablation.

Image Processing and Data Analysis. Images were processed by using ImageJ. They were cropped, rotated, and their contrast and brightness were manually adjusted. Bleb-shape analysis was performed on transmitted-light pictures by using MATLAB (The Math Works) (see *Supplementary Materials and Methods* in the *SI Appendix* for details) .

ACKNOWLEDGMENTS. We thank G. Charras, S. Grill, C. P. Heisenberg, J. Howard, A. Oates, J. Prost, C. Sykes, I. M. Tolic–Norrelykke, and the members of the Paluch lab, particularly A. G. Clark, for critical reading of the manuscript and fruitful discussions. We thank the Max Planck Institute Molecular Cell Biology and Genetics (MPI-CBG) Fluorescence-Activated Cell Sorting Facility for help with the apoptosis controls; the MPI-CBG Light Microscopy Facility for development of the laser-ablation setup and for help with microscopy; and R. Chisholm (Northwestern University, Chicago, IL) for the kind gift of the RLC-GFP plasmid. This work was supported by the Polish Ministry of Science and Higher Education from science funds for the years 2006–2009, by the Max Planck Society, by the Institut Curie/ Centre National de la Recherche Scientifique, and by University Paris VI.

1. Morone N, et al. (2006) Three-dimensional reconstruction of the membrane skeleton at the plasma membrane interface by electron tomography. *J Cell Biol* 174: 851–862.
2. Bray D, White JG (1988) Cortical flow in animal cells. *Science* 239:883–888.
3. Tokumitsu T, Maramorosch K (1967) Cytoplasmic protrusions in insect cells during mitosis in vitro. *J Cell Biol* 34:677–83.
4. Bereiter-Hahn J, Lück M, Miebach T, Stelzer H, Vöth M (1990) Spreading of trypsinized cells: Cytoskeletal dynamics and energy requirements. *J Cell Sci* 96:171–188.
5. Mercer J, Helenius A (2008) Vaccinia virus uses macropinocytosis and apoptotic mimicry to enter host cells. *Science* 320:531–535.
6. Mills JC, Stone NL, Erhardt J, Pittman RN (1998) Apoptotic membrane blebbing is regulated by myosin light chain phosphorylation. *J Cell Biol* 140:627–636.
7. Charras G, Paluch E (2008) Blebs lead the way: How to migrate without lamellipodia. *Nat Rev Mol Cell Biol* 9:730–736.
8. Trinkaus JP (1973) Surface activity and locomotion of Fundulus deep cells during blastula and gastrula stages. *Dev Biol* 30:68–103.
9. Friedl P, Wolf K (2003) Tumour-cell invasion and migration: Diversity and escape mechanisms. *Nat Rev Cancer* 3:362–374.
10. Sahai E, Marshall CJ (2003) Differing modes of tumour cell invasion have distinct requirements for Rho/ROCK signalling and extracellular proteolysis. *Nat Cell Biol* 5:711–719.
11. Blaser H, et al. (2006) Migration of zebrafish primordial germ cells: A role for myosin contraction and cytoplasmic flow. *Dev Cell* 11:613–27.
12. Fackler OT, Grosse R (2008) Cell motility through plasma membrane blebbing. *J Cell Biol* 181:879–884.
13. Charras GT, Hu CK, Coughlin M, Mitchison TJ (2006) Reassembly of contractile actin cortex in cell blebs. *J Cell Biol* 175:477–90.
14. Yoshida K, Soldati T (2006) Dissection of amoeboid movement into two mechanically distinct modes. *J Cell Sci* 119:3833–44.
15. Cunningham CC (1995) Actin polymerization and intracellular solvent flow in cell surface blebbing. *J Cell Biol* 129:1589–1599.
16. Sheetz MP, Sable JE, Döbereiner HG (2006) Continuous membrane-cytoskeleton adhesion requires continuous accommodation to lipid and cytoskeleton dynamics. *Annu Rev Biophys Biomol Struct* 35:417–434.
17. Paluch E, Piel M, Prost J, Bornens M, Sykes C (2005) Cortical actomyosin breakage triggers shape oscillations in cells and cell fragments. *Biophys J* 89:724–733.
18. Mitchison TJ, Charras GT, Mahadevan L (2008) Implications of a poroelastic cytoplasm for the dynamics of animal cell shape. *Semin Cell Dev Biol* 19:215–23.
19. Kruse K, Joanny JF, Jülicher F, Prost J, Sekimoto K (2004) Asters, vortices, and rotating spirals in active gels of polar filaments. *Phys Rev Lett* 92:078101.
20. Kruse K, Joanny JF, Jülicher F, Prost J, Sekimoto K (2005) Generic theory of active polar gels: A paradigm for cytoskeletal dynamics. *Eur Phys J E Soft Matter* 16: 5–16.
21. Evans E, Yeung A (1989) Apparent viscosity and cortical tension of blood granulocytes determined by micropipet aspiration. *Biophys J* 56:151–160.
22. Hochmuth RM (2000) Micropipette aspiration of living cells. *J Biomech* 33:15–22.
23. Kimura K, et al. (1996) Regulation of myosin phosphatase by Rho and Rho-associated kinase (Rho-kinase). *Science* 273:245–248.
24. Wallar BJ, Alberts AS (2003) The formins: Active scaffolds that remodel the cytoskeleton. *Trends Cell Biol* 13:435–46.
25. Charras GT, Yarrow JC, Horton MA, Mahadevan L, Mitchison TJ (2005) Non-equilibration of hydrostatic pressure in blebbing cells. *Nature* 435:365–369.
26. Charras GT, Coughlin M, Mitchison TJ, Mahadevan L (2008) Life and times of a cellular bleb. *Biophys J* 94:1836–53.
27. Thoumine O, Cardoso O, Meister JJ (1999) Changes in the mechanical properties of fibroblasts during spreading: a micromanipulation study. *Eur Biophys J* 28:222–234.
28. Lipowsky R, Sackmann E (1995) *Structure and Dynamics of Membranes*. (Elsevier, Amsterdam).
29. Pasternak C, Spudich JA, Elson EL (1989) Capping of surface receptors and concomitant cortical tension are generated by conventional myosin. *Nature* 341:549–551.
30. Dai J, Ting-Beall HP, Hochmuth RM, Sheetz MP, Titus MA (1999) Myosin I contributes to the generation of resting cortical tension. *Biophys J* 77:1168–1176.
31. Schwarz EC, Neuhaus EM, Kistler C, Henkel AW, Soldati T (2000) Dictyostelium myosin IK is involved in the maintenance of cortical tension and affects motility and phagocytosis. *J Cell Sci* 113:621–633.
32. Carlier MF, Ressad F, Pantaloni D (1999) Control of actin dynamics in cell motility. Role of ADF/cofilin. *J Biol Chem* 274:33827–33830.
33. Sun HQ, Yamamoto M, Mejillano M, Yin HL (1999) Gelsolin, a multifunctional actin regulatory protein. *J Biol Chem* 274:33179–33182.
34. Krieg M, et al. (2008) Tensile forces govern germ-layer organization in zebrafish. *Nat Cell Biol* 10:429–436.
35. Lang T, et al. (2000) Role of actin cortex in the subplasmalemmal transport of secretory granules in PC-12 cells. *Biophys J* 78:2863–2877.
36. Hanakam F, Albrecht R, Eckerskorn C, Matzner M, Gerisch G (1996) Myristoylated and non-myristoylated forms of the pH sensor protein hisactophilin II: Intracellular shuttling to plasma membrane and nucleus monitored in real time by a fusion with green fluorescent protein. *EMBO J* 15:2935–2943.
37. Wu HW, Kuhn T, Moy VT (1998) Mechanical properties of L929 cells measured by atomic force microscopy: effects of anticytoskeletal drugs and membrane crosslinking. *Scanning* 20:389–397.
38. Mahaffy RE, Park S, Gerde E, Käs J, Shih CK (2004) Quantitative analysis of the viscoelastic properties of thin regions of fibroblasts using atomic force microscopy. *Biophys J* 86:1777–1793.
39. Langridge PD, Kay RR (2006) Blebbing of Dictyostelium cells in response to chemoattractant. *Exp Cell Res* 312:2009–2017.
40. Bereiter-Hahn J (2005) Mechanics of crawling cells. *Med Eng Phys* 27:743–753.